Line Profiles from Discrete Kinematic Data

Nicola Cristiano Amorisco

Institute of Astronomy
University of Cambridge

12th April 2012

Motivations

Why Line Profiles?

- Line Profiles constrain the orbital structure;
- break degeneracies: mass profile at the center and at large radii;
- constrain feasible formation scenarios.

Why a new method for discrete data?

- Gauss-Hermite series are best suited for continuous data;
- non-uniform observational uncertainties;
- non-uniform probabilities of membership.

Motivations

Why Line Profiles?

- Line Profiles constrain the orbital structure;
- break degeneracies: mass profile at the center and at large radii;
- constrain feasible formation scenarios.

Why a new method for discrete data?

- Gauss-Hermite series are best suited for continuous data;
- non-uniform observational uncertainties;
- non-uniform probabilities of membership.

1: Limited Sampling

How many tracers are needed?

Limited sampling limits the achievable accuracy.

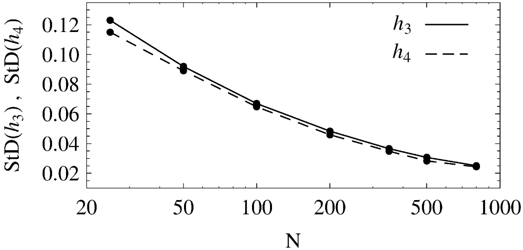

Figure: Accuracy Limits: Standard Deviation for h_3 and h_4 at given sample size N.

For N significantly smaller than 200, noise may be larger than expected signal.

1: Limited Sampling

How many tracers are needed?

Limited sampling limits the achievable accuracy.

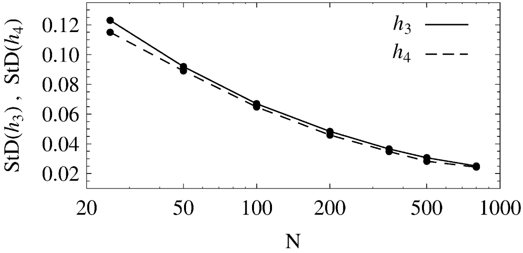

Figure: Accuracy Limits: Standard Deviation for h_3 and h_4 at given sample size N.

For N significantly smaller than 200, noise may be larger than expected signal.

2: Convolution with uncertainties

Attenuation by observational uncertainties.

A tracer $v_i \pm \delta_i$ is associated with the velocity distribution $\mathscr{L} * \mathscr{G}(\delta_i)$, rather than with the intrinsic $\mathscr{L}$.

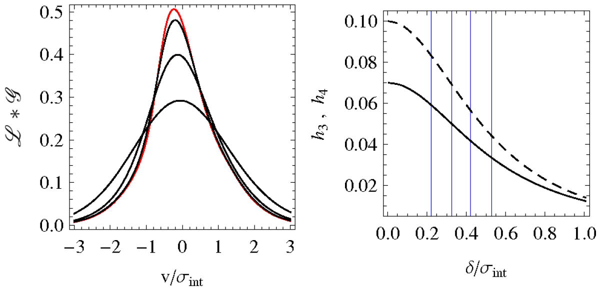

Figure: The effect of observational uncertainties.

On the contrary, a Bayesian implementation directly measures the intrinsic distribution $\mathscr{L}$.

2: Convolution with uncertainties

Attenuation by observational uncertainties.

A tracer $v_i \pm \delta_i$ is associated with the velocity distribution $\mathscr{L} * \mathscr{G}(\delta_i)$, rather than with the intrinsic $\mathscr{L}$.

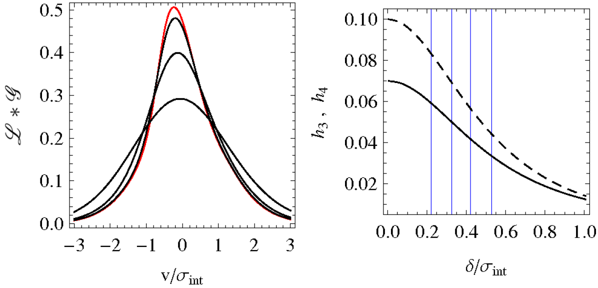

Figure: The effect of observational uncertainties.

On the contrary, a Bayesian implementation directly measures the intrinsic distribution $\mathscr{L}$.

A Bayesian Framework

Using all available information

- the velocities v_i;
- the uncertainties δ_i;
- the probabilities of membership p_i.

$$L(\vec{\Theta}) = \prod_{i=1}^{N} p_i \left[\mathscr{L}(\vec{\Theta}) * \mathscr{G}(\delta_i) \right] (v_i)$$

$$\vec{\Theta} = \{\mu, \sigma\} \cup \vec{\Theta}_{\text{sh}} = \{\mu, \sigma, s, a\}$$

- no binning in velocity space;
- reliable uncertainties for any parameter;
- intrinsic distribution $\mathscr{L}$ recovered.

A Bayesian Framework

Using all available information

- the velocities v_i;
- the uncertainties δ_i;
- the probabilities of membership p_i.

$$L(\vec{\Theta}) = \prod_{i=1}^{N} p_i \left[\mathscr{L}(\vec{\Theta}) * \mathscr{G}(\delta_i) \right] (v_i)$$

$$\vec{\Theta} = \{\mu, \sigma\} \cup \vec{\Theta}_{\rm sh} = \{\mu, \sigma, s, a\}$$

- no binning in velocity space;
- reliable uncertainties for any parameter;
- intrinsic distribution $\mathscr{L}$ recovered.

Symmetric deviations: s

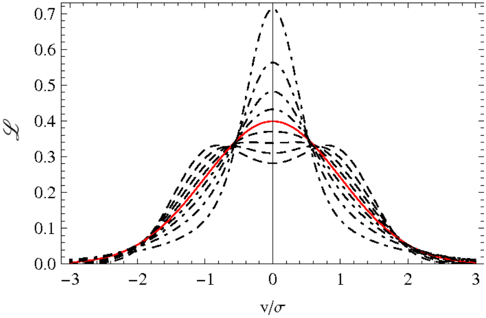

Figure: The symmetric distributions: $\mathscr{L}(s; v)$.

Constructed by using the simple model

$$f(v_r, |\vec{v}_t|) \propto |\vec{v}_t|^{-2s} \exp\left[-\frac{v_r^2 + |\vec{v}_t|^2}{2\sigma_r^2}\right]$$

with anisotropy $\beta = s$ and los direction $\varphi(s)$.

Asymmetric deviations: a

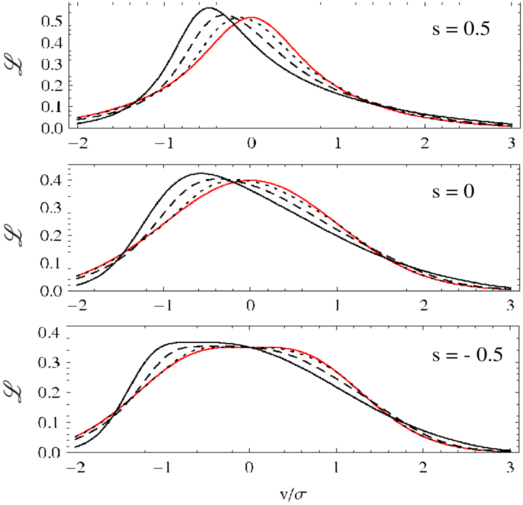

Figure: The asymmetric distributions: $\mathscr{L}(s, a; v)$.

Asymmetry is driven by a suitable tranformation of the symmetric family:

$$\mathscr{L}(s, a; v) \equiv \mathscr{L}(s; X(s, a; v))$$

Performance

Does it work any better?

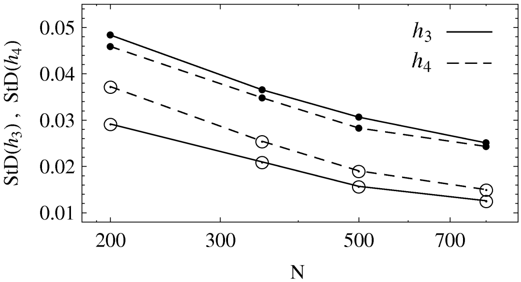

Figure: Comparing Accuracy: Standard Deviation for h_3 and h_4 at a given sample size N.

The relative gain in accuracy is significant even with no observational uncertainties or probabilities of membership.

Assessing Statistical Significance

What if this family is not general enough?

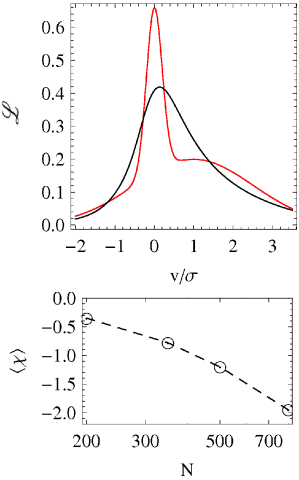

Figure: Testing significance.

Comparing the maximum likelihood

$$\bar{L} = \prod_{i=1}^{N} p_i \left[\mathscr{L}(\vec{\Theta}) * \mathscr{G}(\delta_i)\right](v_i)$$

with the *average* likelihood for the same parameters

$$\langle \prod_{i=1}^{N} p_i \ \mathscr{L} * \mathscr{G} \rangle = \prod_{i=1}^{N} p_i \int \left[\mathscr{L} * \mathscr{G}(\delta_i)\right]^2$$

and the natural scatter induced by sample size

$$\chi = \left(\bar{L} - \langle L \rangle\right) / \mathrm{StD}\left[\langle L \rangle\right]$$

Carina dSph

758 giants with $p_i \geq 0.9$; $\langle\delta\rangle/\sigma \approx 0.53$

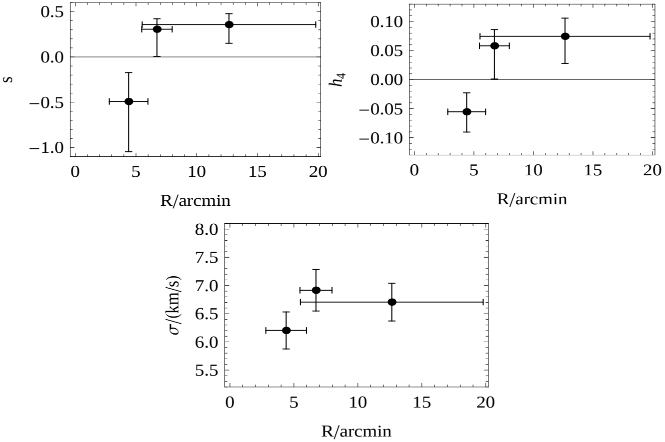

Figure: Profiles in circular annuli for the Carina dSph; $R_h \approx 8.2$arcmin.

Sextans dSph

424 giants with $p_i \geq 0.9$; $\langle\delta\rangle/\sigma \approx 0.42$

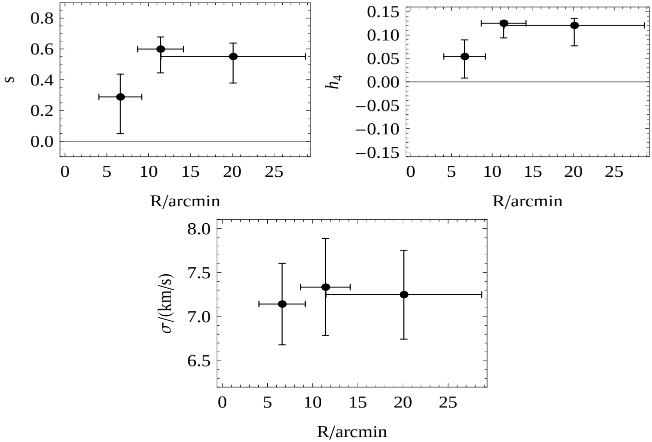

Figure: Profiles in circular annuli for the Sextans dSph; $R_{core} \approx 16.6$arcmin.

Sculptor dSph

1355 giants with $p_i \geq 0.9$; $\langle\delta\rangle/\sigma \approx 0.33$

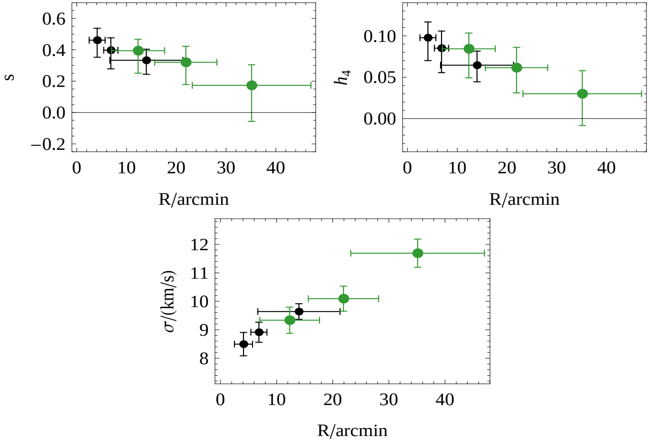

Figure: Profiles in circular annuli for the Sculptor dSph; $R_h \approx 11.3$arcmin. Data from Starkenburg et al. 2010 in green.

Fornax dSph

2409 giants with $p_i \geq 0.9$; $\langle\delta\rangle/\sigma \approx 0.22$

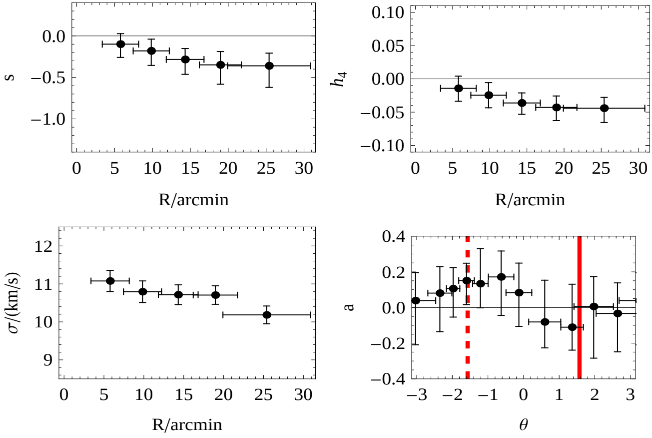

Figure: Profiles in circular annuli for the Fornax dSph; $R_h \approx 16.6$arcmin. Asymmeric deviations in angular sectors $a(\theta)$.

Disentangling Populations

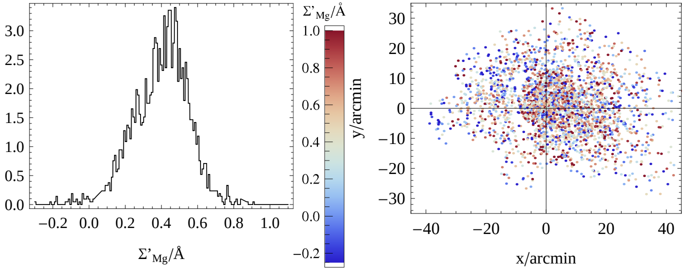

Figure: Metallicity distribution in the Fornax dSph.

$$L = \prod_{i=1}^{N} \left[\sum_j f_j \; p_{R,j}(R_i) \; p_{\Sigma,j}(\Sigma_i) \right]$$

- Plummer density profiles
- Gaussian metallicity distributions

MR - Intermediate - MP

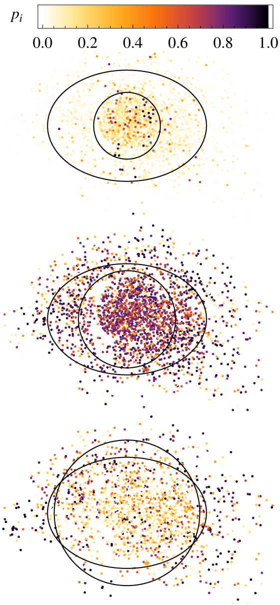

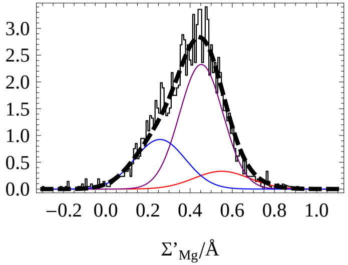

- MR: $R_h \approx 10.5$arcmin, $\langle \Sigma'_{Mg} \rangle \approx 0.55\mathring{A}$, $f \approx .1$
- Int: $R_h \approx 15.3$arcmin, $\langle \Sigma'_{Mg} \rangle \approx 0.45\mathring{A}$, $f \approx .6$
- MP: $R_h \approx 23$arcmin, $\langle \Sigma'_{Mg} \rangle \approx 0.26\mathring{A}$, $f \approx .3$

Kinematics

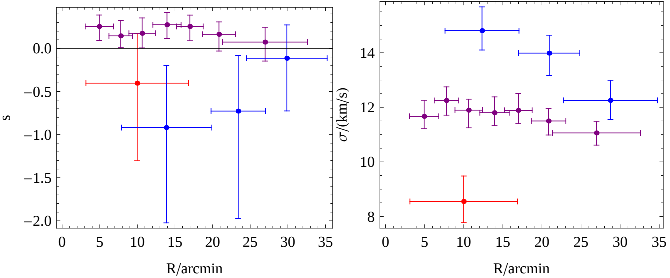

Figure: Kinematics of the disentangled populations.

...and Counter-Rotation

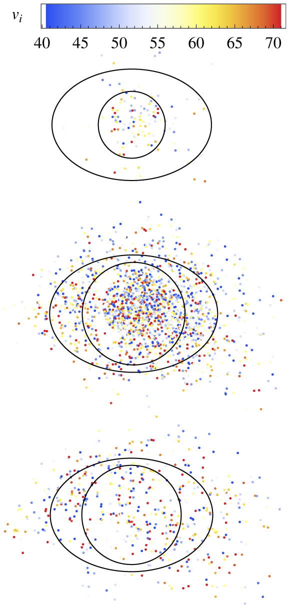

$$L_j \propto \prod_{i=1}^{N} p_i e^{-\frac{\left[v_i-(v_{sys,j}+\Omega_{M,j}x_i+\Omega_{m,j}y_i)\right]^2}{2(\delta_i^2+\sigma_j^2)}}$$

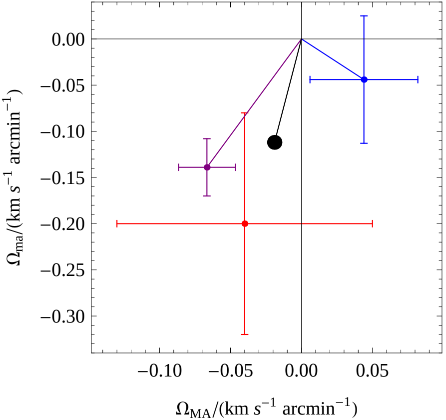

Conclusions

- A **Bayesian framework** for measuring line profiles from discrete kinematic data avoids any binning in velocity space;
- All available information is properly used and **accuracy can be doubled**;
- Proper probability distributions are required, and a suitable two-parameters family is presented;
- A **statistical device** is set to readily quantify the significance of any fit;
- **Sextans, Carina and Sculptor** show line profiles that are more peaked than Gaussian, pointing towards some radial anisotropy;
- **Fornax** is different, containing both a ‘radial’ intermediate population and a ‘tangential’ metal-poor population;
- These two sub-populations are **counter-rotating**, possibly confirming previous indications of a merger.

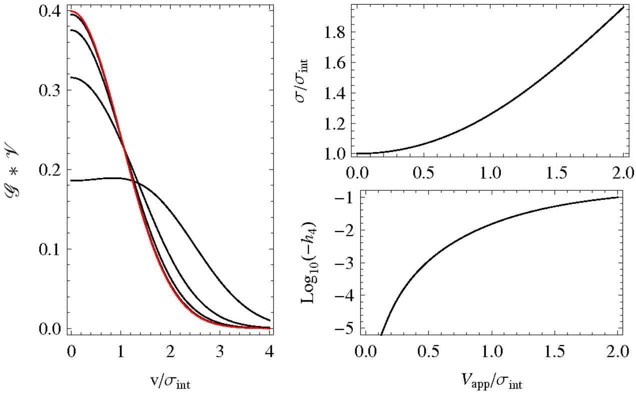

Figure: The effect of apparent rotation on circular annuli.

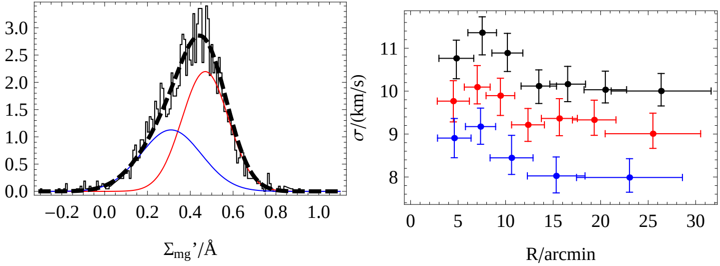

Figure: 'Unstable' kinematics for the 2-pop division in the Fornax dSph.

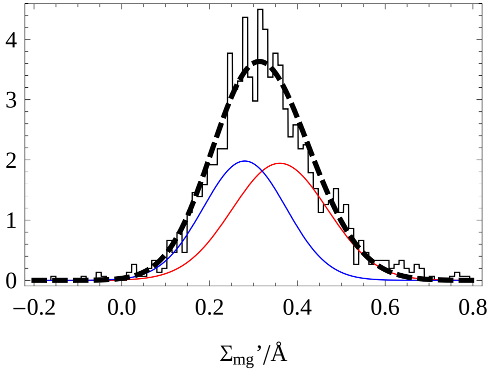

Figure: Metallicity distribution in the Sculptor dSphs.